NASA TM X-67946

NASA TECHNICAL MEMORANDUM

NASA TM X-67946

NONLINEAR, NONLAMINAR - 3D COMPUTATION OF ELECTRON MOTION THROUGH THE OUTPUT CAVITY OF A KLYSTRON

by L. U. Albers and H. G. Kosmahl
Lewis Research Center
Cleveland, Ohio

TECHNICAL PAPER proposed for presentation at
International Electron Devices Meeting
Washington, D.C., November 11-13, 1971

E-6614

NONLINEAR, NONLAMINAR - 3D COMPUTATION OF ELECTRON MOTION THROUGH THE OUTPUT CAVITY OF A KLYSTRON

by L. U. Albers and H. G. Kosmahl

National Aeronautics and Space Administration
Lewis Research Center
Cleveland, Ohio

The attainment of very high efficiencies, that is overall efficiencies in excess of 60% to 80% from klystrons and TWTs requires the knowledge of accurate electron vector velocities at the end of the rf interaction. This knowledge is not so much of importance for the improvement or more accurate computation of the interaction efficiency as for a realistic and accurate treatment of the spent beams prior to and at their injection into novel depressed collectors. Since at K-band frequencies interaction efficiencies about 50% for klystrons and 40% for TWT are difficult to achieve, application of novel depressed collectors becomes thus mandatory for realization of overall super high efficiencies. Efforts to compute 3D electron motion in klystrons and coupled cavity TWTs are under way at LeRC. This paper deals with the accurate computation of electron motion throughout the output cavity of a klystron amplifier. The computation is based upon the following assumptions:

1. The beam is divided into N axisymmetric discs of equal charge $2\pi I_0/N\omega$ and each disc into R rings of equal charge, $2\pi I_0/\omega NR$.

2. The velocity of each disc, its phase with respect to the gap voltage and its radius at a specified position in the drift tunnel prior to the interaction gap is known from available large signal one dimensional programs.

3. The fringing rf fields are computed from exact analytical expressions derived from the wave equation assuming a known field shape between the tunnel tips at a radius a. (See Fig. 1)

4. The beam is focused by an axisymmetric magnetic fields. Both components of B, that is B_z and B_r are taken into account. The flux at the cathode, ψ_c, is available with the limits $\psi_c = 0$ (Brillouin flow) and $\psi_c = 1$ (fully confined flow).

5. Since this integration does not start at the cathode but rather further down the stream prior to entering the output cavity it is assumed that each electron moved along a laminar path from the cathode to the

start of integration, i.e. that its distance from axis relative to other electrons remained unchanged. It is felt that this assumption is well satisfied for confined flow beams prior to entering the output gap since the motion is still almost entirely in one dimension. The assumption is less good for Brillouin and PPM focused beams, but the only alternative is to extend this complex computation into the cathode region if complete accuracy is demanded.

Discussion of Equations of Motion

All equations are used in dimensionless, form normalized with respect to the tunnel radius a and the dc voltage V_o. (Fig. 2)

In the above equations $\alpha = V/V_o$ designates the normalized rf voltage, $\Theta = \omega t; \xi = z/a; \rho = r/a;$ 2ℓ = gap length, ψ and ψ_c are the fluxes in the beam and the cathode, respectively, ω_{pa} and ω_c are the unreduced plasma and the cyclotron frequencies. φ_ξ and φ_ρ designate the normalized axial and radial Green's space charge fields which will be discussed later in detail. Note that the voltage α is not computed but rather assumed to be known.

The rf field factors G_z, F_z and G_r, F_r are derived exactly from the wave equation. They describe the shape and relative magnitude of the axial and radial fields. For $m = 0$ they are identical with equations obtained first by G. Branch by contour integration of Fourier integrals corresponding to a uniform field in the gap at $r = a$. Because of the use of these exact expressions it is unnecessary to introduce radial and axial coupling coefficients. (Fig. 3)

The Space Charge Fields

The space charge fields are derived from a Green's function potential of a solid cylinder of radius a and is simplified for the case of thin discs and narrow rings, that is assuming that the Bessel function $J_o(\lambda_m \cdot \rho)$ varies only slightly inside the ring and thus may be replaced by its value at the ring's center of charge. It may be seen that for large N and R (small, narrow rings) this is very well satisfied. Because the space charge boundary value problem is solved accurately, there is no need to compute or use the reduced plasma frequency. The expressions for φ_ξ and φ_ρ are as follows. (Fig. 4)

Integration and Results

The integration process deals with a set of N discs per cycle. Each disc has a specified time of injection at the place, z =-5a, a specified initial velocity, and an initial width. Each starting disc is divided

into R cell rings of equal volume and charge. Let N be 20 and R be 3 for the purpose of this discussion. The integration process in this case follows 5 points per disc, the two outermost corner rings and the 3 centroid rings. Each disc will be distorted somewhat as it passes down the tube. It may take more than one cycle to traverse the passage to beyond the shield. Therefore a snapshot may contain more than 20 discs, because two representatives of some disc may be in the channel at the same time. A snapshot for the case of $\alpha = .6$, $\ell/a = 2/3$, and $B = 2.5$ BR at time 320° is shown in Figure 5 with each disc represented by a Kite with 5 points.

The most difficult and important aspect of the computation is an accurate treatment of the dynamic effect of space charge forces on the motion of the individual rings. The method is illustrated in Fig. 6. This method was arrived at after subdividing the source rings and reference rings into many fine subrings and carrying out an exact integration of the space charge forces. This lead to the following 3 simplified schemes illustrated by cases 1,2,3 in Fig. 6. In case (1) there is no overlap in the Z direction. Here the equivalent action may be correctly represented by taking the representative ring of the same cell at a position where the centroid of mass is shifted by a fixed amount toward the reference ring. This fixed amount depends only on the width of the two cells. In case number (2) we have Z overlap but not of the center of mass of the reference cell. Here the correct position of the representative source ring leaves the center of mass unshifted thus reducing the repelling forces. This is equivalent to stating that a violent interaction which would occur in a collision of two points does not occur in continuous charge distributions. In case number (3) there is a Z-overlap of the reference centroid. The correct treatment is to split the source cell into two parts: one is symmetric about the reference centroid, the other is the remainder of the source ring. The symmetric part has no Z effect. The R effect is computed by taking the representative source ring at a position half way from the symmetry line to the edge of the subcell. The remainder has its most representative equivalent ring at its centroid. The contributions are weighed by relative volumes.

Case (4) is a simple extension of the principal used in case (3) to describe the effect of a finite size reference ring in itself: in a continuous distribution of changes there would be no Z effect but a R effect equivalent to Gauss law. Using the methods described above the space charge was calculated for every cell at each time step of 10°. The space charge field associated with the snapshot of Fig. 5 is shown in Fig. 7.

Disc number 3 is near the center of bunch. Its $\mathcal{G}_z$ is zero, its $\mathcal{G}_r$ is maximum. Discs 8 and 19 are at left and right of the bunch with unsymmetric distribution. They experience a $\mathcal{G}_r$ force near dc level and maximum of outward $\mathcal{G}_z$ forces. The antibunch disc number 11 experiences about half of $\mathcal{G}_r$ forces and almost no $\mathcal{G}_z$ forces.

The total effect of the circuit fields, magnetic fields and space charge fields on the motion of the rings were computed until steady state condition were achieved. A movie showing the flow will be shown. There are several features of the flow that should be pointed out: the resulting converging action of the radial gap fields, the divergent action of the shield terminating the focusing field on confined flow and the interesting effect of crossovers and overtaking.

The results show that there is no interception and no substantial crossovers for $\alpha \leq 1$ and confined flow focusing, $B \geq 2 B_{BR}$. The radial velocities remain small being less than 10% of the axial component and minimum V_z is ≈ 0.2. The situation changes, however, as α becomes > 1 and for simple Brillouin focusing. Interception and large radial excursions with deflection angles going above 20° increase rapidly as electrons are slowed down more closely to zero.

ELECTRIC FIELD SHAPE BETWEEN REENTRANT TUNNEL TIPS
A - CONSTANT FIELD; B - "KNIFE EDGE" FIELD; C - ACTUAL FIELD

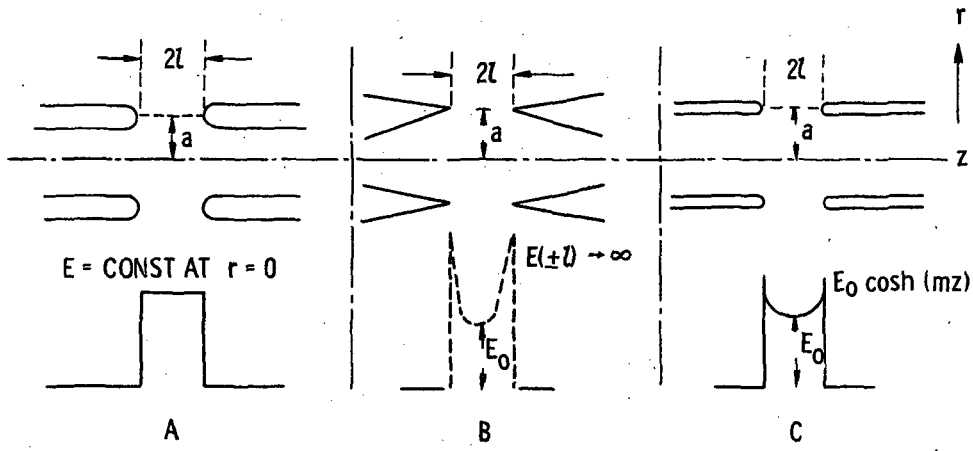

CS-60455

Fig. 1

EQUATIONS OF MOTION

$$\frac{d^2\xi}{d\theta^2} = \frac{\alpha \frac{m\ell}{\sinh(m\ell)}}{4\left(\frac{\ell}{a}\right)(\beta_e a)^2}\begin{pmatrix} G_Z \\ F_Z \end{pmatrix}\sin\theta + \frac{1}{2}\left(\frac{\omega_c}{\omega}\right)^2 \frac{B_\rho(\xi,\rho)}{B_0}\,\frac{\psi(\xi,\rho) - \left(\frac{r_i}{r_e}\right)^2\psi_c}{\psi_a}\,\frac{1}{\rho}$$

$$+ \frac{\pi}{NR}\left(\frac{\omega_{pa}}{\omega}\right)^2 \frac{1}{\beta_e a}\,\mathcal{G}_\xi(\xi,\rho,\xi_0,\rho_0)$$

$$\frac{d^2\rho}{d\theta^2} = \frac{\alpha \frac{m\ell}{\sinh(m\ell)}}{4\left(\frac{\ell}{a}\right)(\beta_e a)^2}\begin{pmatrix} G_R \\ F_R \end{pmatrix}\sin\theta + \frac{1}{4}\left(\frac{\omega_c}{\omega}\right)^2\left(\frac{\psi(\xi,\rho) - \left(\frac{r_i}{r_e}\right)^2\psi_c}{\psi_a}\right)^2\frac{1}{\rho^3}$$

$$- \frac{1}{2}\left(\frac{\omega_c}{\omega}\right)^2 \frac{B_\xi(\xi,\rho)}{B_0}\,\frac{\psi(\xi,\rho) - \left(\frac{r_i}{r_e}\right)^2\psi_c}{\psi_a}\,\frac{1}{\rho} + \frac{\pi}{NR}\left(\frac{\omega_{pa}}{\omega}\right)^2 \frac{1}{\beta_e a}\,\mathcal{G}_\rho(\xi,\rho,\xi_0,\rho_0)$$

CS-60456

Fig. 2

$$G_Z = \begin{cases} \cosh(mz)\dfrac{J_0\left(r\sqrt{k^2+m^2}\right)}{J_0\left(a\sqrt{k^2+m^2}\right)} & -\ll Z < +l \\ -\displaystyle\sum_{n=1}^{\infty}\frac{\lambda_n J_0(\rho\lambda_n)}{p_n J_1(\lambda_n)}\left(\frac{e^{ml}}{p_n - am} + \frac{e^{ml}}{p_n + am}\right) e^{-p_n l/a}\cdot\cosh\frac{p_n z}{a} & \end{cases}$$

$$F_Z = e^{-m|Z|}\ \frac{J_0\left(r\sqrt{k^2+m^2}\right)}{J_0\left(a\sqrt{k^2+m^2}\right)} + \frac{e^{ml}}{2}\sum_{n=1}^{\infty}\frac{\lambda_n J_0\left(\frac{r}{a}\lambda_n\right)}{p_n J_1(\lambda_n)}\ e^{-p_n/a|z|}\left(\frac{e^{p_n(l/a)}}{p_n+m} - \frac{e^{-p_n(l/a)}}{p_n-m}\right)$$

$$+\frac{e^{-ml}}{Z}\sum_{n=1}^{\infty}\frac{\lambda_n J_0\left(\frac{r}{a}\lambda_n\right)}{p_n J_1(\lambda_n)}\ e^{-(p_n/a)|Z|}\left(\frac{e^{p_n(l/a)}}{p_n - am} - \frac{e^{-p_n(l/a)}}{p_n + am}\right) \qquad |Z| > l$$

$$G_R = \sum_{n=1}^{\infty}\frac{J_1\left(\frac{r}{a}\lambda_n\right)}{J_1(\lambda_n)}\ e^{-p_n(l/a)}\ \sinh\left(\frac{p_n Z}{a}\right)\left(\frac{e^{ml}}{p_n - ma} + \frac{e^{-ml}}{p_n + ma}\right)$$

$$-\frac{m}{\sqrt{k^2+m^2}}\ \sinh(mZ)\ \frac{J_1\left(r\sqrt{k^2+m^2}\right)}{J_0\left(a\sqrt{k^2+m^2}\right)} \qquad -<lZ<+l$$

$$F_R = \sum_{n=1}^{\infty}\frac{J_1\left(\frac{r}{a}\lambda_n\right)e^{-p_n(Z/a)}}{J_1(\lambda_n)}\left[\frac{\sinh\left(ml+\frac{l}{a}p_n\right)}{p_n+ma} - \frac{\sinh\left(ml-\frac{l}{a}p_n\right)}{p_n-ma}\right] \qquad Z>l$$

$$F_R = -\sum_{n=1}^{\infty}\frac{J_1\left(\frac{r}{a}\lambda_n\right)e^{-p_n(|Z|/a)}}{J_1(\lambda_n)}\left[\frac{\sinh\left(ml+\frac{l}{a}p_n\right)}{p_n+ma} - \frac{\sinh\left(ml-\frac{l}{a}p_n\right)}{p_n-ma}\right] \qquad Z<-l$$

CS-60458

Fig. 3

GREEN'S FUNCTION POTENTIAL

$$\mathcal{G}_\xi(\xi, \rho, \xi_0, \rho_0) = \sum_{n=1}^{\infty} \sum_{\text{ALL } \rho_0, \xi_0} \frac{J_0(\lambda_n \rho) J_0(\lambda_n \rho_0)}{J_1^2(\lambda_n)} \, e^{-\lambda_n |\xi - \xi_0|} \operatorname{sig}(\xi - \xi_0)$$

$$\mathcal{G}_\rho(\xi, \rho, \xi_0, \rho_0) = \sum_{n=1}^{\infty} \sum_{\text{ALL } \rho_0, \xi_0} \frac{J_1(\lambda_n \rho) J_0(\lambda_n \rho_0)}{J_1^2(\lambda_n)} \, e^{-\lambda_n |\xi - \xi_0|}$$

$J_0(\lambda_n) = 0$

ξ, ρ - COORDINATES OF REFERENCE POINT

ξ_0, ρ_0 - COORDINATES OF SOURCE POINTS

CS-60457

Fig. 4

320° SNAPSHOT OF FLOW IN KLYSTRON

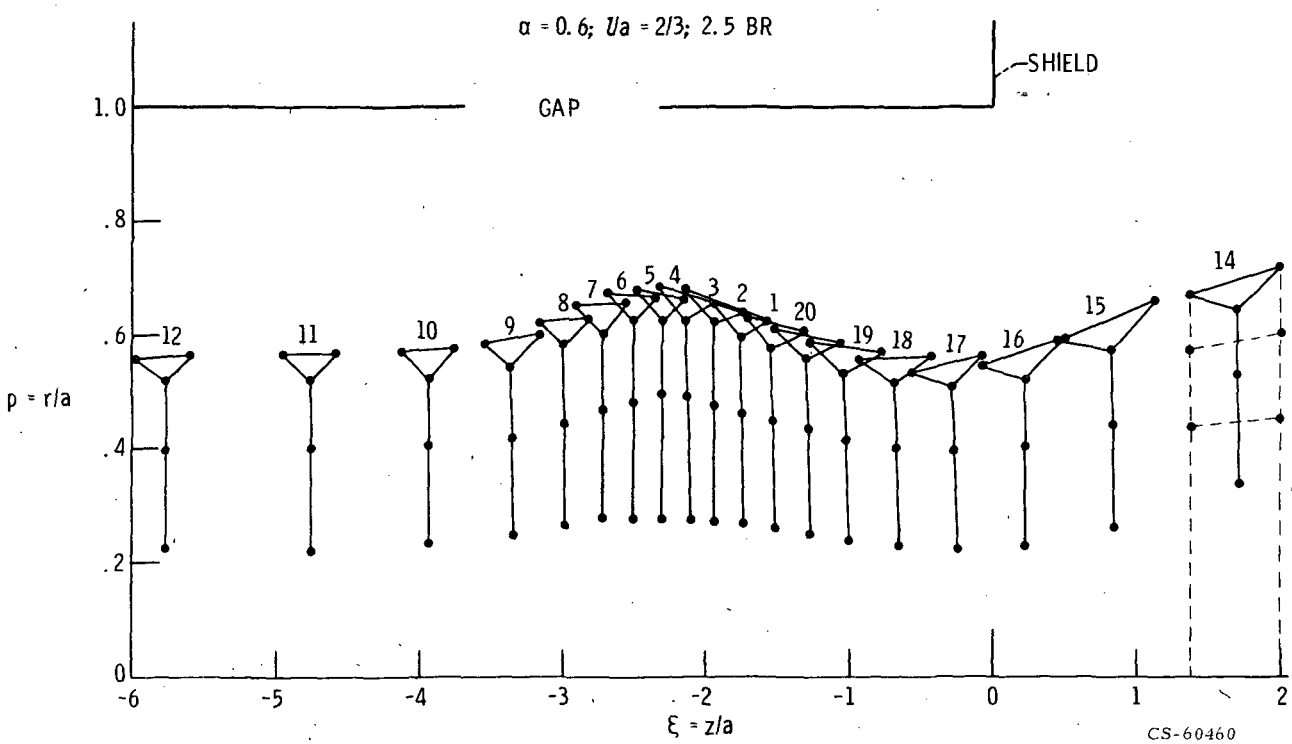

CS-60460

Fig. 5

EFFECT OF SOURCE RING ON REFERENCE RING

CASE 1. - NO Z OVERLAP

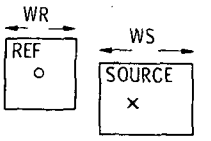

FIXED Z SHIFT DEPENDENT OF WR & WZ

CASE 2. - Z OVERALP, BUT NOT OF REF CENTROID

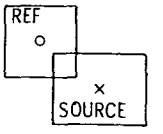

NO SHIFT. EFFECT IS CENTROID TO CENTROID

CASE 3. - Z OVERLAP OF CENTROID

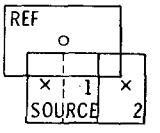

$GR = 0.6\,GR_1 + 0.4\,GR_2$
$GZ = 0.4\,GZ_2$

CASE 4. - EFFECT OF REF RING ON ITSELF

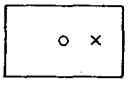

$GR = 0.5\,GR + 0.5\,GR = GR$
$GZ = 0.5\,GZ - 0.5\,GZ = 0$

CS-60459

Fig. 6

GREEN FIELD FOR 320° SNAPSHOT

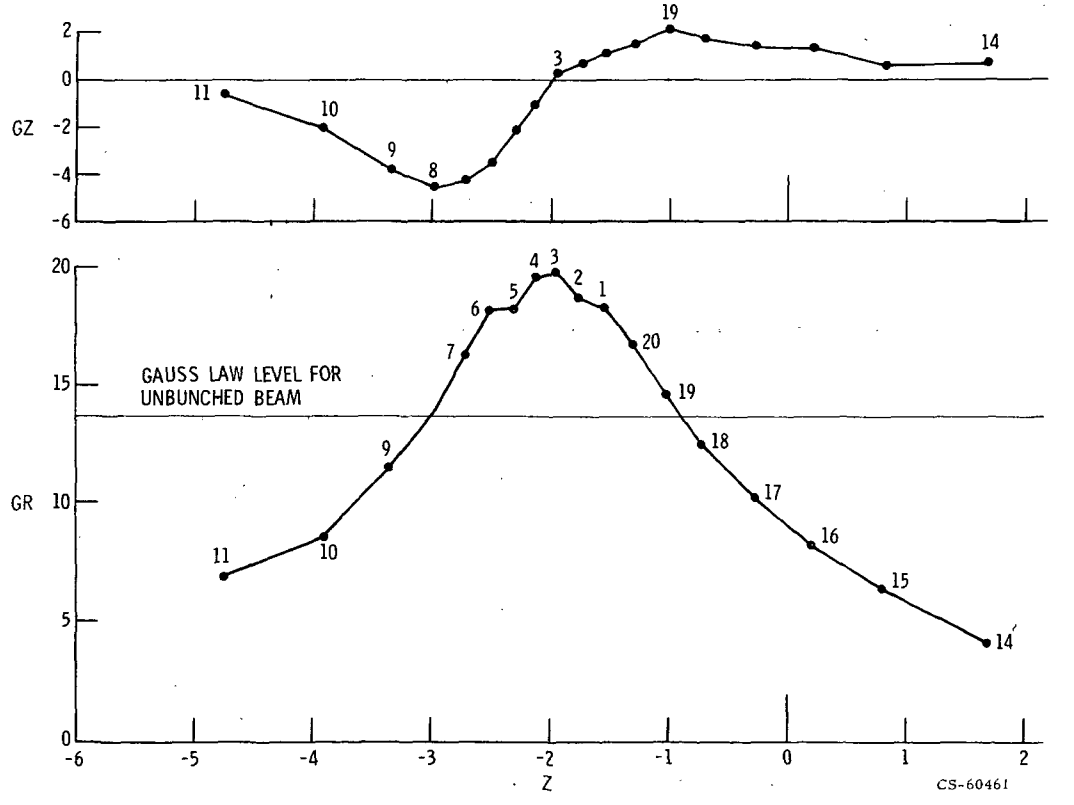

Fig. 7

NASA-Lewis-Com'l